Engineering Structures 221 (2020) 111038

Contents lists available at ScienceDirect

Engineering Structures

journal homepage: www.elsevier.com/locate/engstruct

Description of failure mechanism in placed riprap on steep slope with unsupported toe using smartstone probes

Ganesh H.R. Ravindra[a,*], Oliver Gronz[b], J. Bastian Dost[b], Fjóla G. Sigtryggsdóttir[a]

[a] Department of Civil and Environmental Engineering, S P Andersens veg 5, Norwegian University of Science and Technology, Trondheim 7031, Norway
[b] Department of Physical Geography, Behringstraße/Campus II, Trier University, 54296 Trier, Germany

A B S T R A C T

This article is aimed at investigating the influence of toe support conditions on stability aspects of placed ripraps on steep slopes exposed to overtopping flows. All past experimental model studies investigating placed riprap stability under overtopping conditions have been conducted with ripraps constrained at the toe section. However, ripraps constructed on the downstream slopes of rockfill dams are generally not provided with any form of toe support. Hence, it is of importance from stability and economical standpoints to understand the failure mechanism in placed ripraps with realistic toe support conditions. This article presents findings from experimental overtopping tests conducted on model placed ripraps unsupported at the toe section. Employing Smartstone probes, a new technology in stone movement monitoring, laser measurement techniques and Particle Image Velocimetry (PIV) techniques, detailed description of failure mechanism in placed ripraps under overtopping conditions is presented within this study. Study findings demonstrate sliding as the underlying failure mechanism in placed ripraps with unsupported toes. Further, comparison of experimental results with past findings revealed that placed ripraps with unrestrained toes experience a fivefold reduction in stability, characterized by the critical overtopping magnitude as compared with placed ripraps provided with fixed toe supports. Furthermore, toe support conditions were found to have no effects on either the failure mechanism nor the overall stability of dumped ripraps. Further research is recommended to arrive at well-defined methodologies for design and construction of toe supports for placed ripraps.

1. Introduction

Ripraps are widely used as erosion protection measures against the impacts of currents and waves for various hydraulic structures such as river banks, bridge piers, upstream and downstream slopes of embankment dams, spillways, dykes and breakwaters (e.g. [9,7,30,1,11,25;12]). One application of ripraps within the discipline of dam engineering is to protect the downstream slopes of embankment dams against erosion due to accidental leakage or overtopping events [31]. Ripraps can be broadly classified as either dumped or placed based on the adopted method of construction. Dumped ripraps consist of randomly dumped stones whereas placed ripraps comprise of stones arranged in an interlocking pattern [7]. In order to increase the resistance against erosion from accidental leakage and overtopping events, the downstream slopes of rockfill dams built in Norway are secured with single layer placed ripraps (Fig. 1). The individual riprap stones are to be placed in an interlocking pattern with their longest axis inclined towards the dam [19] and [18]. Many rockfill dams are poised to be upgraded in the near future due to enforcement of more stringent dam safety regulations. This in turn necessitates refurbishment of placed ripraps constructed on these dams. Hence, it is of relevance from stability and economical standpoints to better understand the stability aspects of placed ripraps under overtopping conditions and this forms the primary focus of this study.

Investigation of stability aspects and failure mechanisms in placed ripraps is an intricate task as the failure process is influenced by multitudes of parameters. Factors such as riprap material properties, interlocking effect generated between the individual riprap elements, frictional forces setup at the riprap-filter interface, toe support conditions and overtopping flow magnitude and directionality can have significant influence in discerning the failure characteristics. Placed ripraps exposed to overtopping can undergo failure in several forms such as sliding of the riprap structure, erosion of individual elements leading to exposure of the underlying filter, toe scouring and 2D deformations leading to structural failure. Hence, understanding of these various failure mechanisms is essential to achieve efficient design of these structures.

Available literature describing the stability aspects of placed ripraps under overtopping conditions is rather limited as compared with the extensive research database available with respect to design and construction of dumped ripraps. Notable contributors to the research area of placed riprap design are Hiller et al. [7], Peirson et al. [21], Dornack [2], Sommer [26] and Larsen et al. [13]. An in-depth literature review into the state of the art in placed riprap design is presented within Hiller

* Corresponding author.
E-mail addresses: ganesh.h.r.ravindra@ntnu.no (G.H.R. Ravindra), gronz@uni-trier.de (O. Gronz), s6jodost@uni-trier.de (J.B. Dost), fjola.g.sigtryggsdottir@ntnu.no (F.G. Sigtryggsdóttir).

https://doi.org/10.1016/j.engstruct.2020.111038
Received 23 November 2019; Received in revised form 10 June 2020; Accepted 29 June 2020
Available online 07 July 2020

Nomenclature

a, b, c	longest, intermediate and shortest axes lengths of riprap stones respectively
C_u	coefficient of uniformity
d_i	riprap stone diameter corresponding to i% finer
$d_{i,f}$	filter stone diameter corresponding to i% finer
H_p	height of the horizontal platform
L_s	riprap chute length
n	number of discharge steps
N	number of riprap stones per unit riprap surface area
P	packing factor
q_c	critical unit discharge
q_i	unit discharge at i^{th} step
q_m	combined discharge capacity of the pumps
S	slope (V: H)
t	time
u, v, w	orthogonal Smartstone axes
w_p	width of the horizontal platform
x, y, z	coordinate axes for riprap
α_u, α_v, α_w	respective angles between the u, v, w axes and the gravity vector.
β	angle of a-axis of riprap stones with respect to the slope
ρ_s	density of riprap stones
$\rho_{s,F}$	density of filter stones
Δq	discharge steps
Δt	time interval

et al. [7]. Majority of these past experimental model studies have been aimed at comprehending the underlying 1D failure mechanism in placed ripraps exposed to overtopping flows on mild to moderately steep slopes, S = 0.125 (1:8) to 0.50 (1:2). Furthermore, Hiller et al. [7] conducted experimental overtopping tests on model placed ripraps to analyse the 1D failure mechanism in placed ripraps on a steeper slope, S = 0.67 (1:1.5). These studies concluded that unidirectional stone displacements along the chute direction leading to formation of a gap at the upstream section of the riprap was the underlying failure mechanism in placed ripraps. Also, Hiller et al. [7] stated that placing riprap stones in an interlocking pattern resulted in significant stability gain as compared to randomly dumped riprap. Furthermore, Ravindra et al. [24] continued the experimental research conducted by Hiller et al. [7] to assess 2D failure mechanism in placed ripraps on steep slopes S = 0.67 (1:1.5). Ravindra et al. [24] concluded progressive stone displacements in 2D resulting in buckling like deformation of the riprap structure as the underlying failure mechanism in placed ripraps with restrained toes.

All past studies investigating stability aspects of placed riprap under overtopping conditions have been carried out with ripraps constrained at the toe section with fixed toe support structures. In large-scale practical applications, toe sections of ripraps could be supported employing several toe stabilization techniques. Commencement of riprap construction from a trench excavated into the rock foundation at the toe section, placement of larger size stones at the toe section, increasing the size (volume) of the toe section, and toe blocks of concrete anchored to the foundation with rockbolts or similar, represent some of the toe stabilization measures. Fixed toe support entails enhanced resistance against sliding at the riprap toe section. However, a field survey of existing state of toe support conditions for placed ripraps constructed on several Norwegian rockfill dams was conducted by Ravindra et al. [23] and the study findings demonstrated that none of the surveyed ripraps were currently provided with well-defined toe support measures. Majority of placed riprap toe sections were found to be either lying on bare rock surfaces or buried underneath moderate amounts of soil cover (Fig. 1). Furthermore, several past studies investigating rockfill dam and riprap stability aspects under overtopping conditions such as Morán et al. [17], Jafarnejad et al. [8], Javadi and Mahdi [10] and Morán and Toledo [16] have demonstrated toe section of rockfill dams and ripraps as a critical location for initiation of progressive dam failure. Thus, conducting experimental overtopping investigations on model placed ripraps with realistic toe support conditions is of significance to obtain representative findings concerning the stability aspects of placed ripraps exposed to overtopping flows. This would also facilitate evaluation of the validity of findings from past research works describing stability of placed ripraps under overtopping conditions.

Fig. 1. Placed riprap constructed on Dam Oddatjørn, Suldal, Norway.

This article presents findings from experimental overtopping tests conducted on model placed ripraps unsupported at the toe section. This study is aimed at investigating the influence of toe support conditions on stability aspects of placed ripraps on steep slopes exposed to overtopping flows. Using Smartstone probes[5], a new technology in stone movement monitoring, laser measurement techniques and Particle Image Velocimetry (PIV) techniques, detailed description of failure mechanism in placed ripraps unsupported at the toe is presented within this study. Furthermore, results from this investigation are evaluated against past findings describing stability of placed ripraps exposed to overtopping.

2. Experimental setup and testing program

2.1. Physical model description

A conceptual 1:10 model setup comprising of a single-layered placed riprap section of width w = 1 m and chute length of L_s = 1.8 m constructed over a base frame inclined at a steep slope of 1:1.5 (S = 0.67) was originally designed and constructed by Hiller [6] at the hydraulic laboratory of NTNU, Trondheim, Norway. The setup was designed assuming Froude similarity. This experimental testing facility was further employed in past studies investigating stability aspects of placed ripraps on steep slopes such as Hiller et al. [7] and Ravindra et al. [24]. However, this model consisted of a fixed metallic toe support structure fastened to the base frame at the downstream end of the riprap chute providing resistance against sliding of the riprap structure. A modified version of the model setup originally designed by Hiller [6] was adopted in the present study, wherein the fixed toe support structure was replaced with a horizontal platform at the downstream extremity of the riprap chute to facilitate construction of placed riprap models with unrestrained toes (Fig. 2). The modifications to the

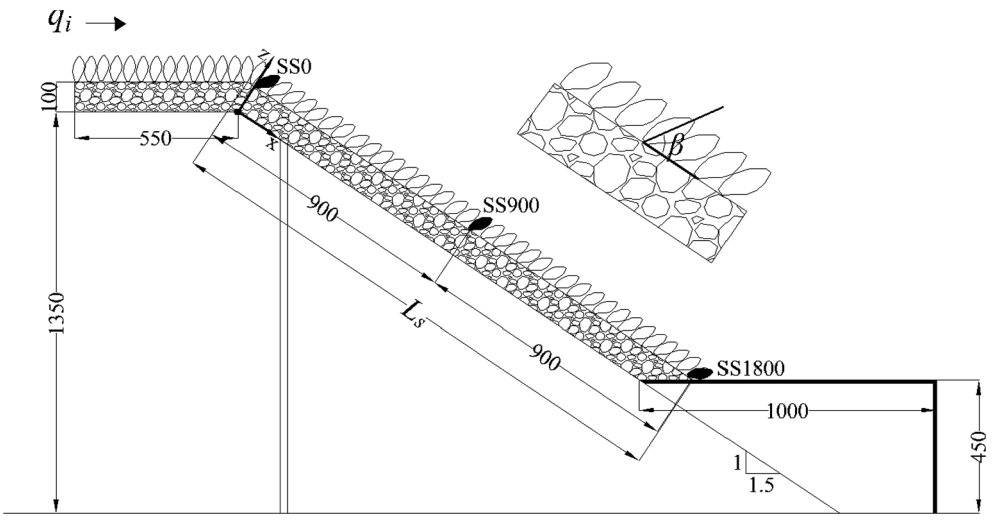

Fig. 2. Illustration of experimental setup of model placed riprap with chute length of L_s = 1.8 m along with portrayal of inclination angle (β) of a-axis of the stones with respect to the chute direction (All measurements in mm). The riprap stones mounted with the smartstone probes are represented as SS_x with x representing distances to the respective stones from the origin along the x-direction.

experimental rig were so designed as to maintain the original dimensioning of the riprap structure as used in past studies such as Hiller et al. [7] and Ravindra et al. [24] to enable comparison of experimental findings.

The model setup was constructed within a 25 m long, 2 m high and 1 m wide horizontal flume. Discharge to the flume was supplied by pumps with a combined capacity of $q_m = 0.4\ m^2\ s^{-1}$. The pumps were equipped with Siemens Sitrans Mag 5000 (Nordberg, Denmark) discharge meters and controlled by valves [7] and [24]. The test setup consisted of a base frame comprising of a 0.55 m long horizontal crest and a 2.43 m long chute along the flow direction, inclined at $S = 0.67$ (1:1.5) (Fig. 2). A horizontal platform with height $H_p = 0.45$ m and width $w_p = 1$ m was coupled with the base frame to facilitate placement of ripraps with unrestrained toes (Fig. 2). The platform also helped elevate the downstream end of the riprap against the flume bottom to avoid backwater effects. This is considering that that the focus of the investigation was on erosion of riprap due to overtopping and not failure due to scour development at the transition to the tail water zone. The surface of the horizontal platform was covered with a layer of geotextile to provide realistic friction for the toe stones. The model setup was located sufficiently downstream of the inflow section to ensure calm flow conditions upstream of the test ripraps [24].

For the construction of model ripraps, quarry stones of rhyolite [14] with median diameter of $d_{50} = 0.057$ m and density of $\rho_s = 2710\ kg\ m^{-3}$ were used. The median riprap stone size was computed as $d_{50} = (abc)^{1/3}$ averaged over a sample size of 500 stones, where a, b and c represent the longest, intermediate and shortest axis respectively. The respective axes lengths were manually measured employing a calliper and the mean values were recorded as $a = 0.091$ m, $b = 0.053$ m and $c = 0.038$ m. The riprap stones could be considered angular to sub-angular with average $a\ b^{-1} = 1.7$ and uniformly graded with $C_u = d_{60}\ d_{10}^{-1} = 1.17$. Test ripraps were placed on a 0.1 m thick filter layer comprised of geotextile and angular stones of size $d_{50,f} = 0.025$ m and density $\rho_{s,f} = 3050\ kg\ m^{-3}$. The dimensions of the filter and the riprap were chosen in accordance with guidelines offered by the Norwegian Water Resources and Energy Directorate [18].

Overtopping tests were carried out with both placed and dumped ripraps to better understand the fundamental differences and similarities in failure mechanisms between the two structures (Fig. 3). The test ripraps covered the 0.55 m long horizontal crest and the 1.8 m long chute. Placed riprap models were constructed by manual placement of stones in an interlocking pattern commencing at the toe, progressing upstream to the crest (Fig. 3a). The individual riprap stones were deliberately placed with the longest axis (a-axis) inclined at $\beta \approx 60^\circ$ with respect to the chute bottom and at an inclination of $\beta \approx 90^\circ$ on the horizontal crest to account for practical considerations (Fig. 2) [15]. It should be noted that the last row of riprap stones, which constitute the toe of the riprap were placed flat on the horizontal platform ($\beta \approx 0^\circ$) (Figs. 2 and 3). Subsequent rows of stones were placed at incremental inclinations to attain the required stone inclinations of $\beta \approx 60^\circ$. This was also in alignment with the findings from field surveys of riprap toes conducted by Ravindra et al. [23], wherein mean placement inclinations (β) for the toe stones were found to be much lower in comparison with those for the riprap stones. Further, single layer dumped ripraps were constructed by randomly dumping the riprap stones on the slope with arbitrary orientations and without any interlocking pattern (Fig. 3b).

Riprap stones placed on the horizontal crest cannot be considered part of the riprap structure. This is considering that the riprap stones placed on the steep slope are exposed to higher destabilizing forces as compared with stones on the horizontal crest [24]. Hence, riprap stones

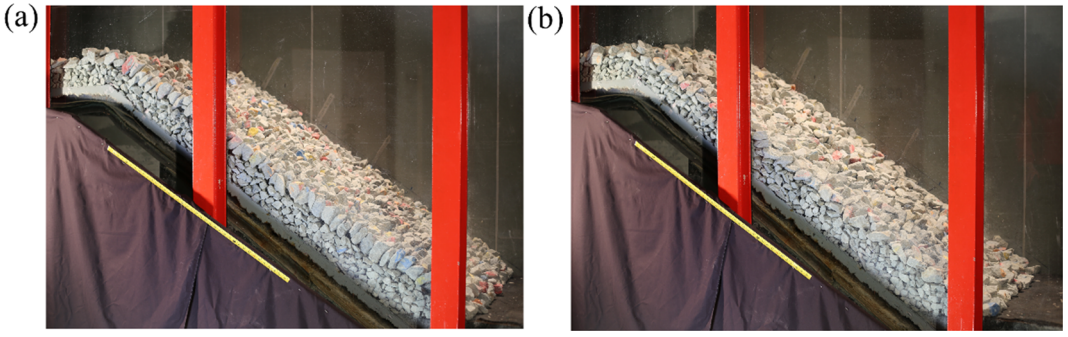

Fig. 3. Depiction of experimental model setups with (a) placed and (b) dumped ripraps at the hydraulic laboratory of NTNU, Trondheim, Norway.

covering the 0.55 m horizontal crest are not considered part of further analysis in this study and are incorporated within the model setup to simulate realistic flow transitions from the crest onto the riprap structure.

The packing factor (P) originally defined by Olivier [20] has been utilized in several past investigations concerning placed riprap stability to obtain a quantitative measure of density of riprap stone placement as this can have an impact on overall riprap stability. This has further been incorporated within this study as Eq. (6).

$$P = \frac{1}{N\, d_{50}^{2}} \tag{6}$$

where N represents the number of stones per m^2 surface area of the riprap and d_{50} signifies the median stone size. P is lower for a placed riprap compared to dumped riprap [7].

2.2. Laser traverse system

A 3D laser traverse system situated overhead of the model setup was employed to measure location co-ordinates of select riprap stones. The traverse operated within a 3D Cartesian coordinate system with its origin situated at the transition from the horizontal crest to the inclined chute (Fig. 2). The x-axis was aligned in a direction parallel to the chute (33.7° to the flume bottom) pointing in the downstream direction and the z-axis was set perpendicular to the chute. Measurement accuracies were ± 0.1 mm and ± 1 mm in the x and z-directions respectively. Stone displacements were considered only along the x and z-directions as any possibility of encountering lateral flows prompting stone displacements in the y-direction was ruled out [7] and [24].

2.3. Smartstone probes

Monitoring of stone movements prior to and during structural collapse of the riprap is of importance to gain better understanding of the underlying failure mechanism. However, due to flow aeration in the model and the sudden nature of riprap collapse, conventional stone displacement measurement techniques could not be used for monitoring stone motions during the tests. To obtain quantitative descriptions of stone displacement in the tested riprap structures prior to and during riprap failure, new technology in stone displacement monitoring named as Smartstone probes (Smartstone probe v2.1) (Fig. 4), developed at the University of Trier, Germany has been used within this study.

It is an advancement from the former version that was presented by Gronz et al. [5]. The current probe features thre triaxial sensors manufactured by Bosch Sensortec GmbH. The BMI 160 [4] is placed centric within the Smartstone probe and holds the acceleration sensor (ACC) and the gyroscope (GYR). The measuring range of the current ACC is increased from ± 4 g to ± 16 g (1 mg noise) within the present Smartstone version from the earlier probe version 1.1. The GYR records rotational velocity within the range of ± 2000 $^{\circ}s^{-1}$ (0.04 $^{\circ}s^{-1}$ noise). Additionally, it contains the magnetic sensor (MAG) BMC 150 [4], which has not been put to use in this study.

Motion data and the corresponding time stamps are stored on a 1 MB internal memory. Data can be read out wirelessly by means of active radio frequency identification (active RFID) technology. Moreover, the entire communication between a computer and the sensor is carried out via RFID and an USB-gateway. A software with graphical user interface (GUI) allows for easy handling and control of different sensor settings (sampling rate, record threshold etc.). The current probe version is encased in a 50 mm long and 10 mm wide plastic tube that is sealed at the ends with plastic plugs. Due to the non-metal casing, an internal antenna can be installed, which makes the probe more practicable under experimental conditions. Energy for recording and data exchange is supplied by a standard 1.5 V button cell (type AG5). The Smartstone probe prototype was designed and manufactured in cooperation with the company Smart Solutions Technology GbR, Germany and is still under further development.

The length of the plastic tube is variable, so the battery can be adapted to a specific application. The button cell is small resulting in the length of 50 mm. But its capacity is limited to one run of the experiment and should thus be replaced after each run. Data transmission after the experimental run further contributes towards exhaustion of battery life. For other applications with larger stones, a longer plastic tube and an AAAA battery could be used, allowing for more than one year of active waiting for trigger. The memory size allows for up to 8 min of constant movement with 100 Hz sampling rate. Commencement of data acquisition is marked by exceedance of stone movements over a user-defined threshold.

In order to equip select riprap stones with Smartstone probes within the present study, cylindrical holes of diameter 10 mm and length 50 mm were drilled within the stones utilizing a mechanical drill. The drill holes were aligned with the longest stone axes (a-axes). The probes were encased in watertight rubber envelopes and mounted within the cylindrical drill holes. The openings were further sealed using waterproof sealing agents.

Three riprap stones were mounted with Smartstone probes and placed within the test ripraps at the crown, the center and at the toe sections of the riprap structure. Stones implanted with the probes are herein referred to as ‘Smartstones’. This was to monitor stone movements at these locations as this could provide details regarding initiation and progression of riprap failure. The respective stones were identified as SS_0, SS_{900} and SS_{1800} (Fig. 2) respectively with the indices representing the distance to the respective stones from the origin along the x-direction. The selected stones were located along the centreline of the flume (y = 0.5) to address concerns of wall effects.

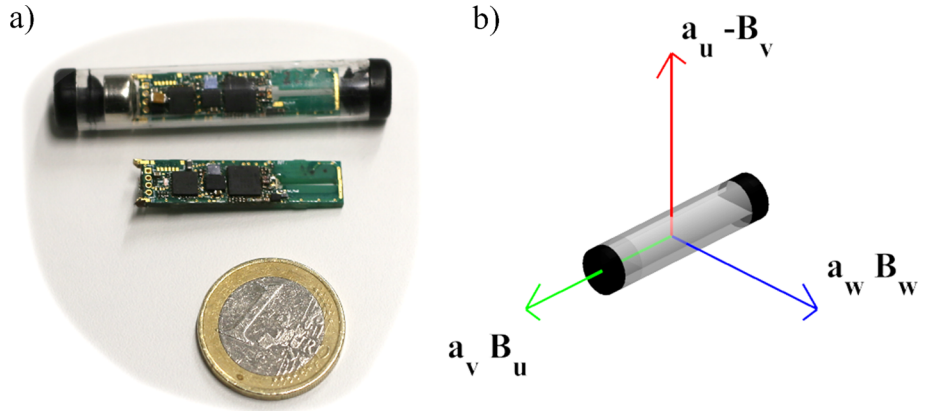

Fig. 4. (a) The Smartstone probe in a plastic tube with button cell on the left end and the circuit board with sensors underneath. (b) The probe’s coordinate system.

2.4. Particle Image Velocimetry (PIV)

High-speed video footages of the overtopping tests were recorded over the course of the experimental testing program. The video footages were in turn subjected to Particle Image Velocimetry (PIV) analysis to enable cross corroboration of investigation results. PIV analysis allows for estimation of the velocity distribution in image pairs. The direction and the velocity of particles in these image pairs result from cross-correlation functions. The tool PIVlab [28,29,27,3], which is available for MATLAB was implemented to carry out the analysis. The recorded video footages were split into images and were further stored as single greyscale images within the PIV toolbox using MATLAB's rgb2gray function. The distance between the bars at the flume's sidewalls was used to calibrate distance. Besides this, PIVlab's standard parameterization was used in the analysis.

2.5. Testing methodology

In previous studies such as Hiller et al. [7] and Ravindra et al. [24], overtopping tests on model placed and dumped ripraps with toe support were conducted by exposing the riprap structures to incremental overtopping flows in step-wise increments of $\Delta q = 0.02–0.05\ m^2\ s^{-1}$ over specific time intervals of $\Delta t = 1800$ s. However, due to limitations with the Smartstone probes with respect to battery life and inbuilt memory, adoption of similar testing methodology as employed within previous investigations to conduct extended overtopping tests was not possible within the present study. Hence, testing methodology was modified to accommodate the limitations of the probes. This was done also considering changes in the behavior of placed riprap models with unsupported toes concerning deformations and critical discharges.

To begin with, several pilot overtopping tests with placed and dumped ripraps were conducted without incorporation of the Smartstone probes. Details from illustrative tests, P01 and D01 conducted with placed and dumped ripraps respectively are presented in Table 1. The pilot tests on model ripraps were carried out by exposing the riprap structures to incremental overtopping with discharge steps of $\Delta q = 0.02\ m^2\ s^{-1}$. The initial overtopping discharge magnitude was set to $q_i = 0.02\ m^2\ s^{-1}$ as this was the minimum required flow to achieve submergence of the riprap stones. The discharge levels were maintained constant over regular time intervals of $\Delta t = 1800$ s.

The 3D location co-ordinates of several marked stones were measured in between overtopping steps using the 3D laser traverse system as described within Hiller et al. [7] and Ravindra et al. [24]. This procedure was further repeated over n discharge steps until ultimate riprap collapse was achieved (q_c). The critical overtopping magnitudes for placed and dumped ripraps were consistently found to $q_c = 0.06$ and $0.04\ m^2\ s^{-1}$ respectively. The pilot tests provided measurements regarding riprap deformations prior to failure initiation and also, probable critical discharges for initiation of irreversible riprap collapse.

Further, for tests conducted with placed and dumped ripraps implanted with Smartstone probes, the riprap structures were directly exposed to the critical discharge (q_c) levels obtained from the pilot tests in order to achieve riprap failure in the shortest possible time. This was to obtain measurements regarding the motion of riprap stones during riprap collapse, also accommodating limitations of the Smartstone probes. Furthermore, video footages from the tests were captured using a high-speed camera stationed next to the viewing gallery of the flume. In essence, the adopted testing procedure results in measurements describing motion of the riprap stones prior to and during riprap collapse thereby providing a comprehensive description of the underlying failure mechanisms in the tested placed and dumped ripraps.

3. Results

3.1. Stability aspects

Details regarding the experimental testing program are presented within Table 1. The table presents particulars regarding construction and testing procedures adopted for experiments conducted on placed (P01 - P06) and dumped (D01 - D03) ripraps. The critical overtopping discharge levels for initiation of irreversible riprap failure (q_c) were found to be higher for placed ripraps as compared with dumped ripraps. Unraveling riprap failures were found to be initiated at overtopping discharge magnitudes of $q_c = 0.06\ m^2\ s^{-1}$ and $0.04\ m^2\ s^{-1}$ respectively for placed and dumped ripraps (Table 1). This ratio of critical discharge values between placed and dumped ripraps was hence found to be 1.5.

Further, the 2D deformations within placed riprap structures were analyzed with respect to incremental overtopping discharge magnitudes using laser measurements of location co-ordinates of six marked stones. Reference is made to Ravindra et al. [24] for further details regarding the analysis procedure. Analysis results revealed that the marked riprap stones placed on the riprap chute underwent only minor displacements along and normal to the chute direction (x and z axes respectively) prior to initiation of progressive riprap failure. Further, the toe stones placed on the horizontal platform experienced insignificant downstream displacements along the platform surface. Furthermore, no definite correlations were found between the stone displacements and the overtopping discharge magnitudes.

3.2. Initiation and progression of riprap failure

As stated previously, the Smartstone probes were employed within this study to better understand the mechanisms of failure initiations and progression in placed and dumped ripraps with unsupported toes. Also, Particle Image Velocimetry (PIV) analysis using the recorded video footages (provided as a supplementary video file) were also conducted to further validate results derived from the Smartstones. Cumulative results from the analyses conducted implementing these two techniques are presented herein.

Referring to Table 1, tests P02 - P06 and D02 - D03 were carried out with Smartstones on placed and dumped ripraps respectively. Prior to exposure of the riprap structure to overtopping, the Smartstone probes were configured to record measurements of accelerations and orientations using the in-built accelerometer and gyroscope. The data acquisition protocol was set to commence upon reaching a threshold trigger acceleration of 48 mg, as this would limit excessive recording of minor stone vibrations prior to failure initiation thereby preserving battery life and memory. Data acquisition rates for the probes were set to 100 Hz. Measurements from Smartstone probes implanted within stones identified as SS_0, SS_{900} and SS_{1800} (Fig. 2) were further time synchronized to enable comparison of measurements between sensors in time to gain a better understanding of stone displacements at different locations within the riprap structures.

Table 1
Description of the experimental testing procedure.

Test	P_c (-)	q_i ($m^2\ s^{-1}$)	n (-)	Δt (s)	q_c ($m^2\ s^{-1}$)
P01*	0.53	0.02–0.06	3	1800	0.06
P02	0.53	0.06	1	–	0.06
P03	0.54	0.06	1	–	0.06
P04	0.48	0.06	1	–	0.06
P05	0.49	0.06	1	–	0.06
P06	0.52	0.06	1	–	0.06
D01*	0.91	0.02 – 0.04	2	1800	0.04
D02	0.83	0.04	1	–	0.04
D03	0.74	0.04	1	–	0.04

* Pilot tests conducted without incorporation of the Smartstone probes.

3.2.1. Phases of riprap failure

Detailed analysis of the accelerometer and gyroscope data revealed that riprap failure takes place in uniquely identifiable phases. To illustrate the sequence of events leading up to and further progressing as total riprap collapse, depictions of stone acceleration and orientation measurements for an overtopping test conducted on a model placed riprap are presented as Fig. 5). Recorded measurements from the Smartstone placed at the riprap crest (S_0 from Fig. 2) from test P05 are portrayed in Fig. 5. Further, the individual phases of stone motions within the time series are labelled with capital letters. To better illustrate the failure mechanism, a video footage demonstrating the initiation and progression of placed riprap failure has been provided as a supplementary video file along with the article.

Phase A: Upon exposure to overtopping flow, the water level upstream of the model increases and eventually overtops the riprap structure. The start of Phase A ($t = 0$) represents the trigger point of the probe subsequent to which the probe initiates the data recording protocol. That is, at $t = 0$, the water flow reaches a magnitude that results in accelerations of the sensor-equipped stone that exceed the pre-set acceleration threshold of 48 mg. This acceleration can be a result of minor changes in stone inclination by fractions of a degree, as a change of inclination changes the fraction of gravity measured along each probe axis. This effect can be considered a consequence of vibrations generated due to initial flow attack on the stone. The threshold trigger acceleration was set to 48 mg within our tests basing on results from pilot tests. This can be considered an important parameter as setting a high threshold would lead to the risk of missing out on data gathering during riprap failure and a low threshold could result in filling up of the internal sensor memory prior to riprap failure. Hence, it was of essence to conduct pilot studies to discern the optimal threshold acceleration magnitude based on the experimental conditions. Further, the concerned riprap stone was found to not undergo major displacements during the remainder of phase A. Similar observations were made for Smartstones placed at the centre (S_{900}) and at the toe of the riprap (S_{1800}).

Before the next phase is described, influence of gravity on the probe's measurements should be explained. Under stationary conditions, acceleration measurements from the probes along each axis only shows a fraction of the gravitational acceleration, depending on the angle between this axis and the gravity vector (pointing vertically downwards). Let α_u be the angle between the probe u-axis and the gravity vector, α_v be the angle between the v-axis and the gravity vector and α_w be the angle between the w-axis and the gravity vector. If the stone is not moved at all, acceleration measurements from the probes along these axes will then show $a_u = \cos(\alpha_u) \cdot 1$ g, $a_u = \cos(\alpha_v) \cdot 1$ g and $a_w = \cos(\alpha_w) \cdot 1$ g. Resulting from this, small changes in the sensor's orientation are visible in changing levels of readings of the three axes. Further, if the sensor is moved, the acceleration readings will represent the sum of the gravity induced accelerations and those induced due to stone movements. Furthermore, there is only one possible scenario that results in zero measurements from the probes along all the measurement axes: free fall.

Phase B: The hydrodynamic drag and lift forces generated by incremental overtopping flows reach higher magnitudes resulting in strong vibrations as can be seen from the accelerometer plot in Fig. 5. The mean deviation in accelerations from the average acceleration values are between 0.095 g and 0.102 g for the u and w probe axes respectively. The impinging flow forces and the resulting vibrations further lead to small reorganizations of the stones within the riprap structure, as demonstrated by minor changes in stone inclinations. These are visible within the acceleration plots for the u and w axes (the blue and red lines) presented in Fig. 5. These are on different levels prior to phase B and almost on the same level after phase B. This entails that the stone underwent rotation along the u-w plane to attain a final configuration for Phase C. This conclusion can also be further corroborated through inspection of the video footage that reveals that during phase B, the riprap layer in its entirety undergoes slight compaction and the stones experience changes in orientation, tilting towards the downstream direction. The Smartstone placed at the centre (S_{900}) of the riprap displays a similar behaviour. However, the stones placed at the toe (S_{1800}) do not appear to experience significant displacements or rotations during this phase. These observations are also in line with

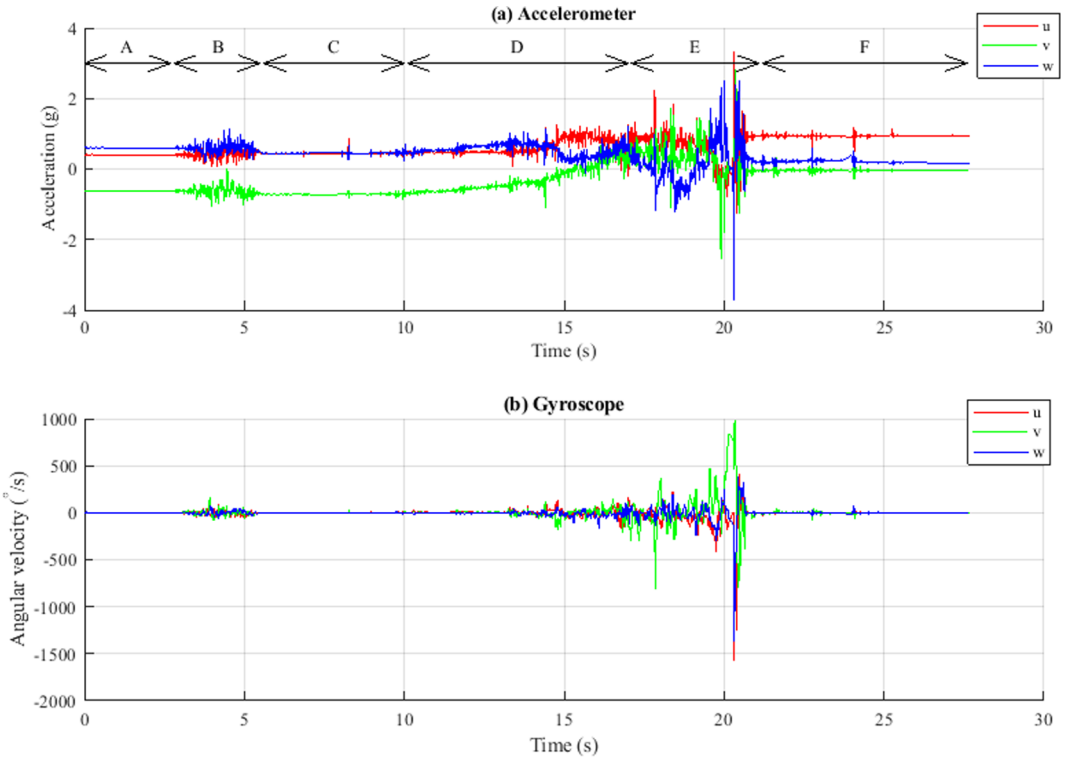

Fig. 5. Depictions of (a) accelerometer and (b) gyroscope measurements from the Smartstone placed at the riprap crest (S_0) from test P05.

findings from section 3.1 wherein 2D displacements of select stones prior to riprap collapse were monitored by adopting the laser traverse system. Only minor displacements along and normal to the chute direction (x and z axes respectively) were recorded prior to failure initiation.

Phase C: After this initial readjustment phase leading to compaction of the riprap structure, there is a phase of relative rest with only occasional single small spikes in the acceleration data. In this phase, the overtopping flow magnitude is gradually increasing.

Phase D: The failure begins quite slowly during several seconds with a tilting of the stones in the riprap layer. This tilting is visible by the changing levels of the different acceleration time series. It can be observed that the absolute values at the v axis (green line) gradually decrease while the w axis values increase (blue line). Thus, the sensor's end indicated by the blue w axis moves downwards. This effect is also documented in the video as the whole top layer tilts within this phase of failure initiation.

Phase E: Initiation of progressive collapse of the riprap structure, which will be further discussed in greater depth using more detailed depictions (Fig. 6).

Phase F: The riprap stones further collapse to form a pile on top of the horizontal platform. The pile is still overrun by water, resulting in small spikes in measurements. The pile is continually undergoing rearranged as a consequence of flow attack after a pause of several seconds.

In Fig. 6, the collapse (phase E of Fig. 5) is shown in detail. In the accelerometer plot, the resultant (black line) and the filtered resultant (thick grey line) are overlaid. The resultant is the length of the vector $u + v + w$ (without sign). If the sensor is not moved, the resultant is always 1 g (gravity). In any other case, the value will be the sum of gravity and the accelerations resulting due to displacements of the stone. In free fall and without aerodynamic drag, resultant acceleration of 0g is expected. Further, as sporadic spikes in data impede the interpretation of the resultant, the filtered resultant is also added in Fig. 6. For the resultant, a high pass has been applied (removes gravity) and afterwards a low pass has been applied (smooths spikes). The high pass removes low frequencies and constant components from the time series. This is mainly the gravity induced fraction of the signal as long as the stone is not moving or only vibrating or moving at constant velocity. Afterwards, a low pass has been applied, which removes single peaks and high frequency noise from the signal. In the filtered resultant, stationary periods, accelerations and decelerations are much easier to identify as a sequence.

The collapse begins slowly at approximately 17.5 s. The filtered resultant acceleration plot shows increasing magnitudes of up to 0.37 g at 18.4 s. Afterwards, it decreases to almost 0 g, indicating a constant collapse velocity. At 19.7 s, the filtered resultant increases again as this represents the instant when the Smartstone reaches the pile which has been formed on the horizontal platform. It seems to rebound from the pile at 20 s, as a small period of free fall is visible afterwards between 20.2 and 20.3 s (u, v and w axes show nearly 0 g). This assumption is also supported by the strong acceleration peaks observed subsequently, when the stone impacts with the pile once again. During the rebound, the stone rotates quickly at 800°s^{-1}, which lasts for 0.2 s. Finally, the stone remains somewhere on or within the pile. The orientation is different from before the collapse, as the different acceleration levels in the axes in phases A and F in Fig. 5 indicate.

The acceleration and the gyroscope measurements were subjected to further analysis to derive displacement velocities of the Smartstone during riprap failure. The initial position and the gyroscope data were used to account for stone rotations within the acceleration data. Using integration of the acceleration values, a velocity time series was obtained. The resulting velocity plot is shown in Fig. 7. The probe-equipped stone is seen to be gradually accelerated, reaching velocities of up to 0.66 m s^{-1} at t = 19.7 s. When the stone reaches the pile formed on the horizontal platform, rapid decelerations can be observed.

A brief summary of salient features of the different phases involved in the failure process of placed ripraps as detailed previously has been presented within Table 2 for easy reference.

The velocities derived from Smartstone data should be further

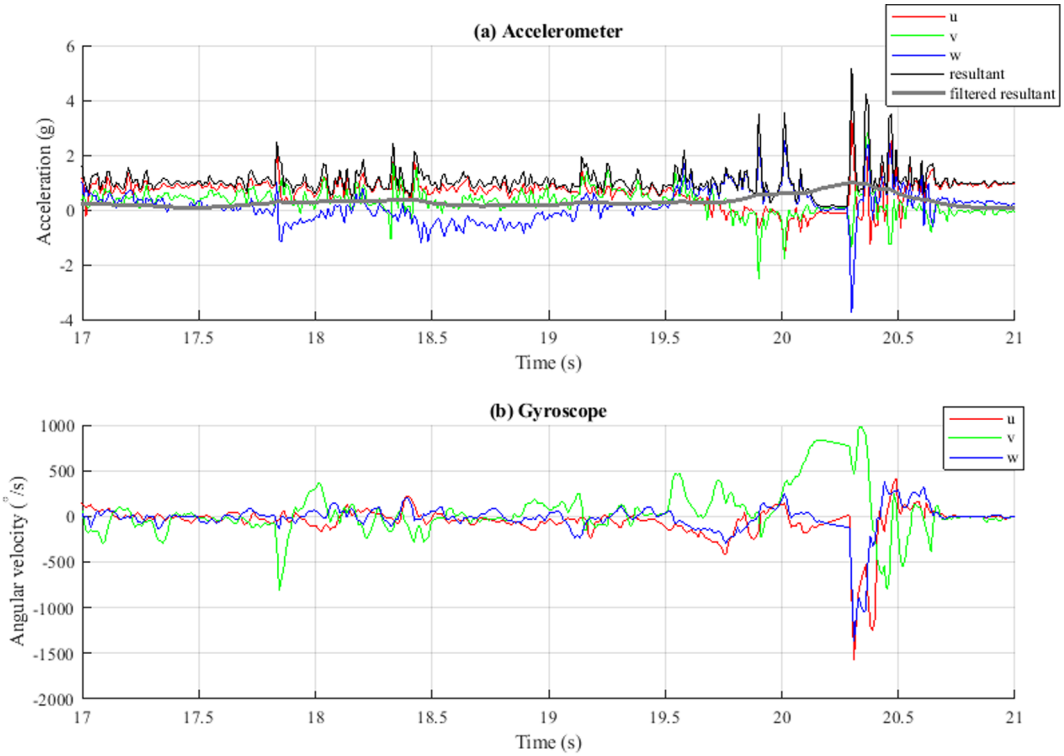

Fig. 6. Detailed plots of (a) accelerometer and (b) gyroscope measurements from the Smartstone placed at the riprap crest (S_0) from test P05 during total riprap collapse (Phase E).

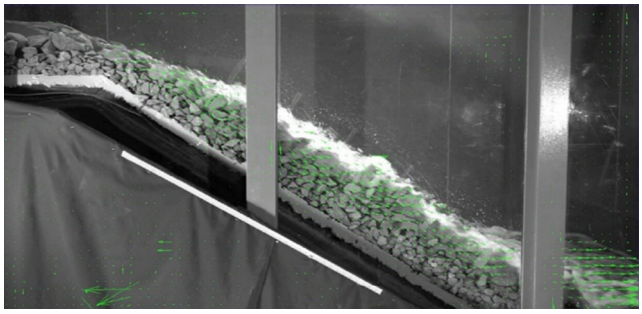

Fig. 7. Single frame from PIV analysis. Green vectors indicate direction of flow and the length indicate the velocity (From Test P05).

confirmed using different techniques. To accomplish this, Particle Image Velocimetry (PIV) analysis was conducted on the video footage (Supplementary video file) to obtain velocity distributions during the overtopping test. For each frame, the estimated velocities are stored in a matrix for the horizontal component and a second matrix for the vertical component. Fig. 7 shows a sample frame, where the matrix cell's resultant is represented by vectors. A cell next to the bar approximately in the center of the frame and in the middle of the stone layer was selected. The peak of the time series of the PIV-derived velocities (Fig. 8) in this cell were compared to Smartstone derived velocities. In all runs that were compared, excellent correlation between the Smartstone derived maximum velocities and the PIV derived peak velocities were observed. Deviations between PIV and Smartstone velocities ranged between 0.01 and 0.06 m s^{-1}.

In total, three runs of placed ripraps and three runs of dumped ripraps were examined. The observations in these two groups were found to be similar within each group and also the differences between the groups are obvious. The general findings are: Placed ripraps collapse was found to occur more abruptly than dumped ripraps. The peak velocities were also found to be higher (between 0.66 and 1.008 m s-1) for placed ripraps as compared with velocities computed for dumped ripraps (between 0.31 and 0.52 m s-1). Also, placed riprap acceleration time series show more frequent and higher magnitude peaks, while the gyroscope time series show less rotations. This in turn entails that placed ripraps are characterized by high degree of vibrations within the riprap structure and that placed ripraps collapse as a unit in the sense that the whole riprap layer slides down the slope as a unified structure. However, for dumped ripraps, less acceleration peaks were visible and significantly higher stone rotations were recorded by the gyroscope. This further suggests that dumped riprap failures entail lower degree of vibrations and that the failure progresses randomly with erosion of individual stones from the slope.

4. Discussions

4.1. Description of the failure mechanism

Cumulative analysis of data obtained from different independent measurement techniques such as laser tracking, Smartstones and video records provide a comprehensive description of the underlying failure mechanism in placed ripraps with unsupported toes. As demonstrated by the gyroscope and the accelerometer data sets, placed riprap stones experience minor degree of reorientations and displacements along the downstream chute direction following initial exposure of the riprap structure to overtopping flows (Phases A and B in Fig. 5). These observations were further supported by inspection of the video footage, which revealed that during phase B, the riprap layer as a whole undergoes compaction and reorganization along the downstream direction. Furthermore, monitoring of stone displacements using the 3D laser traverse system also support these findings as minor displacements along the x and z axes were recorded prior to failure initiation. These can be explained as a consequence of the manual stone placing efficiency during construction of the riprap models. Although individual stones are manually placed one after another, the riprap structure could be loosely packed with intermediate voids. Hence, upon initial exposure to overtopping, the incremental hydraulic drag and lift forces and the resulting vibrations lead to rearrangements of the individual stones wherein the riprap structure undergoes compaction to fill the voids. Similar observations describing compaction of placed riprap structures upon exposure to initial low magnitude overtopping flows were also documented within Ravindra et al. [24].

Further during phase C (Fig. 5), no displacements or reorientations of the riprap stones were observed. This entails that upon undergoing minor deformations leading to compaction of the riprap structure, the individual stones achieve a stable configuration leading to the formation of a unified structure. This can be explained as due to generation of interlocking forces between the individual riprap stones. With further increments in overtopping magnitude, the riprap structure is exposed to higher destabilizing hydraulic forces. These are in part transferred on to the underlying filter layer as frictional forces. The remainder is directed towards the riprap toe where the static frictional forces setup between the toe stones and the geotextile membrane laid on the horizontal platform increase in magnitude to counter the incremental hydrodynamic forces transferred towards the toe. Furthermore, initiation of riprap collapse marks the point of time at which the magnitude of the impacting hydrodynamic forces exceed the limiting values of the static frictional forces between the toe stones and the horizontal platform. This frictional yield results in displacements of the toe stones and following this event, the riprap structure in its entirety undergoes a progressive slide on the underlying filter layer, further forming a pile on the flume bottom.

Siebel [25], Dornack [2], Sommer [26] and Larsen et al. [13] investigating the 1D behavior of placed ripraps stated that the interlocking of riprap stones allows for the transfer of longitudinal forces

Table 2
Different phases involved in the failure of placed ripraps with unsupported toes.

Phase	Features
A	• Exposure to overtopping leading to submergence of the riprap structure. • The flow forces result in accelerations of the sensor-equipped stone exceeding the pre-set threshold of 48 mg.
B	• Incremental hydrodynamic drag and lift forces lead to strong vibrations. • These result in small reorganizations of the stones within the riprap structure. • The toe stones do not experience significant displacements or rotations.
C	• Period of relative rest during exposure to incremental overtopping.
D	• The failure begins during several seconds with tilting of the stones in the riprap layer.
E	• Initiation and further progression of collapse of the riprap structure.
F	• The riprap stones further collapse to form a pile on top of the horizontal platform. • The pile continually undergoes rearrangements as a consequence of flow attack after a pause of several seconds.

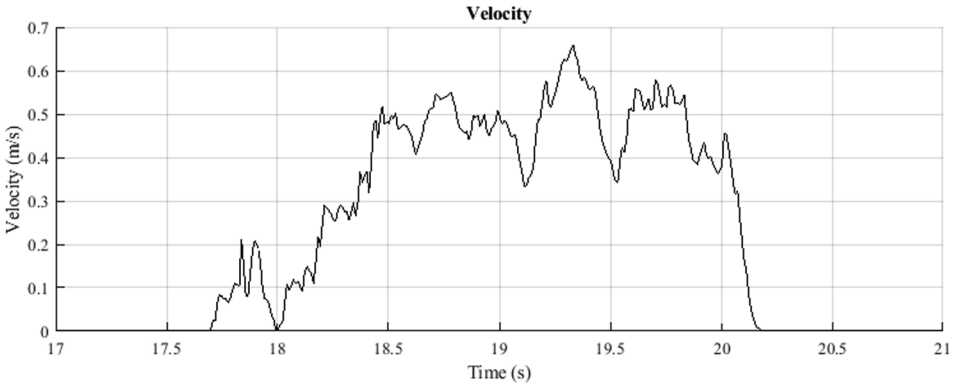

Fig. 8. Smartstone probe derived velocity for Smartstone (SS_0) from Test P05.

within the placed ripraps. They concluded that these forces, when large enough, could either cause sliding or rupture of the riprap layer. This paper describes sliding as the underlying failure mechanism in placed ripraps with unsupported toes. However, Ravindra et al. [24] demonstrated a buckling like structural collapse as the failure mechanism in placed ripraps on steep slopes provided with fixed toe support. Juxtaposition of these two disparate failure mechanisms helps bring out the importance of toe support conditions in discerning the failure mechanism in placed ripraps. In case of a constrained toe structure as adopted in Ravindra et al. [24], the riprap structure is likely to fail as a consequence of structural collapse or buckling as the toe support structure provides unlimited resistance stabilizing the toe, in turn eliminating the possibility of sliding of the riprap structure. Under such conditions, the riprap structure experiences some degree of compaction during initial stages of overtopping exposure and further, following the formation of a unified riprap structure, incremental overtopping flows give rise to development of progressive 2D deformation profiles in ripraps resembling the buckling process in a slender-long column as demonstrated by Ravindra et al. [24]. However, in case of an unrestrained toe, the placed riprap section slides along the steep slope as a result of limited frictional resistance offered at the toe section. Hence, the current investigation explains that the configuration of the toe section of placed riprap as a key factor influencing the overall failure mechanism. Further, Hiller et al. [7] investigated 1D displacement of riprap stones in placed riprap with supported toes and showed that compaction of the riprap structure at the downstream end leads to formation of a gap at the upstream crest of the riprap. However, this was not observed within this study as the limited frictional forces setup at the interface between the toe stones and the horizontal platform do not allow for such a high degree of compaction to occur. The riprap structure experiences sliding failure due to toe yield before any major compaction or 2D deformation of the riprap structure could occur.

It was earlier demonstrated that dumped and placed ripraps are characterized by distinct failure mechanisms when exposed to overtopping. Dumped ripraps were found to go through a surface erosion process where individual stones were eroded by the action of destabilizing turbulent flow forces. This was in contrast to failure initiation in placed ripraps wherein the riprap structure as a whole was found to undergo a slide. This difference in the failure mechanisms can be described as due to the absence of interlocking forces between individual riprap stones. Since dumped ripraps comprise of randomly arranged stones, individual stones are not interlocked with the adjacent elements. When the dumped riprap structure is exposed to overtopping flow forces, the individual stones counter the flow attack primarily through self-weight of the individual elements and the bottom frictional forces generated at the riprap-filter interface. Failure initiation marks the instant at which the magnitude of the destabilizing hydrodynamic forces exceed the resultant of the stabilizing self-weight and the frictional forces. Hence, dumped riprap failure can be stated as the resultant of progressive unraveling erosion of individual riprap elements whereas placed riprap failure entails sudden slide of the entire riprap structure. This also provides an explanation for higher velocities measured for stone displacements in placed ripraps during failure as compared to dumped riprap stones. Placed ripraps experience an instantaneous slide following toe yield wherein the riprap structure moves down the slope as a unit. Whereas dumped riprap failure entails erosion of discreet riprap elements wherein individual stones suffer collisions with one another during the erosion process thereby resulting in loss of kinetic energy. Further, placed riprap failures were found to be initiated at higher overtopping magnitudes as compared with dumped ripraps. As a combined effect of these two causes, placed riprap stones travel on the slope at higher velocities than dumped riprap stones. Furthermore, a similar mode of failure was described for dumped ripraps within Hiller et al. [7] wherein model studies were conducted with placed ripraps provided with fixed toe supports. This in turn suggests that toe support conditions have no effect on the failure mechanism in dumped ripraps exposed to overtopping.

4.2. Importance of toe support for riprap stability

The critical overtopping discharge magnitudes for initiation of riprap collapse (q_c) were found to be $q_c = 0.06\ m^2\ s^{-1}$ and $0.04\ m^2\ s^{-1}$ for placed and dumped ripraps respectively constructed with stones of dimension $d_{50} = 0.057$ m within the present experimental study (Table 1). Considering Froude scaling with a scaling ratio of 1:10, for ripraps built with stones of mean diameter of $d_{50} = 0.57$ m at the prototype scale, the critical overtopping discharges would translate to $q_c = 1.9\ m^2\ s^{-1}$ and $1.3\ m^2\ s^{-1}$ respectively for placed and dumped ripraps with unsupported toes. This in turn entails that placed ripraps unsupported at the toe offer 1.5 times higher stability, characterized by the critical overtopping magnitude as compared with dumped riprap. Past experimental studies conducted on placed riprap models provided with fixed toe supports such as Hiller et al. [7], Peirson et al. [22], Dornack [2] and Larsen et al. [13] have also demonstrated that placed ripraps offer higher stability as compared to dumped riprap, especially at steep slopes. Hiller et al. [7] conducted experimental overtopping investigations with 1: 10 scale model placed ripraps with fixed toe supports constructed with riprap stones of average diameter $d_{50} = 0.057$ m. Hiller et al. (2018a) documented average critical overtopping magnitudes of $q_c = 0.30\ m^2\ s^{-1}$ and $0.04\ m^2\ s^{-1}$ respectively for placed and dumped ripraps ($9.5\ m^2\ s^{-1}$ and $1.3\ m^2\ s^{-1}$ respectively at the prototype scale) resulting in a ratio of average critical discharge values of 7.5. The fivefold reduction in placed riprap stability in terms of average critical overtopping discharge magnitude required to achieve placed riprap from $q_c = 0.30\ m^2\ s^{-1}$ within Hiller et al. [7] to $q_c = 0.06\ m^2\ s^{-1}$ within the present study can be attributed to the absence of a toe support structure. At prototype scales, this would entail a reduction in critical overtopping magnitude from $q_c = 9.5\ m^2$

s^{-1} to 1.9 $m^2\ s^{-1}$. However, dumped riprap stability can be stated as being unaffected by toe support conditions as the critical discharge for failure initiation remained constant at $q_c = 0.04\ m^2\ s^{-1}$ between model setups (1.3 $m^2\ s^{-1}$ at prototype scales). These findings further add to the earlier statement that toe support conditions can have considerable impacts on placed riprap stability and not on the stability aspects of dumped ripraps.

4.3. Smartstones

The Smartstone probes represent state of the art technology in stone movement monitoring. Adoption of this sophisticated technique within the experimental model setup facilitated in obtaining better understanding of the failure mechanisms in placed and dumped ripraps exposed to overtopping. The probes have been found to be versatile and reliable with broad ranging capabilities. A major advantage of the technique is concerning elimination of undesirable effects on flow hydraulics within the model. Results from the present study clearly demonstrate that the Smartstones probes are capable of capturing several important details regarding initiation and progression of failure in ripraps such as acceleration and angular velocities of the stones thereby providing an overarching picture of the underlying failure mechanisms. However, the probes currently face limitations with regards to limited battery life and internal memory capabilities. Further improvements to the probes addressing these limitations could greatly enhance potential for implementation of the probes within practical and experimental applications.

4.4. Limitations and recommendations

- The experimental testing program employed within this study utilizes a distinct setup with placed riprap models built on a steep slope, $S = 0.67$ (1:1.5) with angular stones ($a\ b^{-1} = 1.7$) placed at an angle of $\beta = 60^{\circ}$. Validity of experimental results considering different material properties and construction methods should be studied in future investigations to address scaling concerns and to improve confidence for wide-ranging applicability of study findings.
- The packing factor (P_c) values for the tests incorporated in this study vary within a narrow range of 0.49–0.54 for placed ripraps and hence, detailed evaluation of the influence of P_c on overall placed riprap stability is not possible from this study. Further research in this regard is recommended in future investigations.
- Investigation of impacts of air-entrainment on overall riprap stability is beyond the scope of the present study and inclusion of this as a study parameter in future research works is recommended.
- With respect to scaling of study findings, large-scale overtopping field tests with placed ripraps constructed on rockfill slopes are recommended to evaluate the validity of the observed failure mechanism at larger scales.
- Toe support conditions for placed ripraps have been demonstrated as a key factor influencing the overall failure mechanism. Further research to arrive at design criteria and solutions as well as construction methodologies for riprap toes is highly recommended for future investigations.

5. Concluding remarks

This study adds to the state of the art within the study discipline of placed riprap stability exposed to overtopping conditions. The investigation is aimed at obtaining better understanding of the importance of toe support conditions on stability aspects of placed ripraps through experimental overtopping tests conducted on 1:10 scale model placed riprap structures with unsupported toes constructed on steep slopes of 1:1.5 (vertical: horizontal slope dimensions).

Employing Smartstone probes, the state of the art in stone movement monitoring, detailed description of the underlying failure mechanism in placed ripraps with unsupported toes is presented. Study findings demonstrate sliding as the underlying failure mechanism in placed ripraps with unsupported toes. This was found to be the resultant of limited frictional resistance available at the toe section of the riprap. The sliding failure observed within this study for placed ripraps with unsupported toes was in contrast to the buckling like 2D structural deformations documented within Ravindra et al. [24] for placed ripraps provided with fixed toe supports. Further, comparison of critical discharge magnitudes from the present study with those of Hiller et al. [7] revealed that placed ripraps with unrestrained toes experience a five-fold reduction in stability as compared with placed ripraps provided with fixed toe supports. Further, toe support conditions were found to have no effects on either the failure mechanism or the overall stability of dumped ripraps.

Findings from the present study suggest that toe support conditions can have significant impact on the overall stability aspects of placed ripraps under overtopping conditions. However, recent findings from Ravindra et al. [23] revealed the fact that existing placed ripraps built on rockfill dams are generally not provided with any well-defined form of toe support. Findings from the present study lead to the conclusion that coupling existing riprap structures with toe supports can lead to considerable gain in overall stability. Since multitude of rockfill dams are poised to be upgraded in the near future, arriving at criteria and measures for the toe support design and construction is of significance from placed riprap stability standpoint. Hence, further research addressing this vital feature influencing placed riprap stability is highly recommended.

CRediT authorship contribution statement

Ganesh H.R. Ravindra: Conceptualization, Methodology, Investigation, Writing - original draft, Writing - review & editing. **Oliver Gronz:** Software, Formal analysis, Investigation, Data curation, Visualization. **J. Bastian Dost:** Software, Formal analysis, Investigation, Data curation, Visualization. **Fjóla G. Sigtryggsdóttir:** Conceptualization, Methodology, Writing - original draft, Writing - review & editing.

Declaration of Competing Interest

The authors declare that they have no known competing financial interests or personal relationships that could have appeared to influence the work reported in this paper.

Acknowledgements

The authors acknowledge the financial support offered by HydroCen, Norway. The support and co-operation from Dr. Priska Helene Hiller, NVE, Norway and Prof. Jochen Aberle, TU Braunschweig, Germany in designing the original experimental setup is appreciated. The authors appreciate the assistance of Dr. Andreas Krein, Luxembourg Institute of Science and Technology. The authors would also like to thank the MSc student Malin F Asbølmo for the assistance offered during the experimental testing program.

Appendix A. Supplementary material

Supplementary data to this article can be found online at https://doi.org/10.1016/j.engstruct.2020.111038.

References

[1] Abt SR, Thornton CI, Scholl BA, Bender TR. Evaluation of overtopping riprap design relationships. J Am Water Resour Assoc 2013;49(4):923–37.
[2] Dornack S. Überströmbare Dämme – Beitrag zur Bemessung von Deckwerken aus Bruchsteinen/ Overtopping Dams-Design Criteria for Riprap PhD thesis Technische

Universitat Dresden; 2001.
[3] Garcia D. A fast all-in-one method for automated post-processing of PIV data. Exp Fluids 2011;50:1247–59.
[4] Bosch Sensortech GmbH. “BMC150 and 150”; 2019. URL: https://www.bosch-sensortec.com/bst/products/all_products/bmc150, https://www.bosch-sensortec.com/bst/products/all_products/bmc160, retrieved: 15/Oct/2019.
[5] Gronz O, et al. Smartstones: A small 9-axis sensor implanted in stones to track their movements. Catena 2016;142:245–51.
[6] Hiller PH. Riprap design on the downstream slopes of rockfill dams. Doctoral Thesis. Trondheim: Norwegian University of Science and Technology; 2017.
[7] Hiller PH, Aberle J, Lia L. Displacements as failure origin of placed riprap on steep slopes. J Hydraul Res 2018;56(2):141–55.
[8] Jafarnejad M, Franca MJ, Pfister M, Schleiss AJ. Time-based failure analysis of compressed riverbank riprap. J Hydraul Res 2017;55(2):224–35.
[9] Jafarnejad M, Franca MJ, Pfister M, Schleiss AJ. Design of riverbank riprap using large, individually placed blocks. J Hydraul Eng 2019;145(12):1–12.
[10] Javadi N, Mahdi T-F. Experimental investigation into rockfill dam failure initiation by overtopping. Nat Hazards 2014;74:623–37.
[11] Khan D, Ahmad Z. Stabilization of angular-shaped riprap under overtopping flows. World Acad Sci, Eng Technol, Int J Civil, Environ, Struct, Construct Architectural Eng 2011;5(11):550–4.
[12] Kobayashi N, Jacobs BK. Riprap stability under wave action. J Waterw Port Coastal Ocean Eng 1985;111(3):552–66.
[13] Larsen P, et al. Uberstrombare Damme, Hochwasserentlastung Uber Dammscharten/ Overtoppable Dams, Spillways over Dam Notches. Unpublished report prepared for Regierungsprasidium Karlsruhe Universita; 1986.
[14] Lev V, Anantharamu V. Estimating the elastic properties of mica and clay minerals. Geophysics 2020;85(2). MR83–95.
[15] Lia, Leif, Vartdal EA, Skoglund M, Campos HE. Riprap protection of downstream slopes of rockfill dams-a measure to increase safety in an unpredictable future climate. European club symposium of the international comission on large dams; 2013.
[16] Morán R, Toledo MA. Reserarch into protection of rockfill dams from overtopping using rockfill downstream toes. Can J Civ Eng 2011;38(12):1314–26.
[17] Morán, Rafael, Miguel Á Toledo, Antonia Larese, and Ricardo Monteiro-alves. 2019. “A Procedure to Design Toe Protections for Rock Fi Ll Dams against Extreme Through- Fl Ows.” 195: 400–412.
[18] NVE. Veileder for fyllingsdammer/guidelines for rockfill dams. Norwegian water resources and energy directorate; 2012. 21–25.
[19] OED. Forskrift Om Sikkerhet Ved Vassdragsanlegg (Damsikkerhetsforskriften). Oljeog Energidepartementet; 2009.
[20] Olivier, Henry. Through and overflow rockfill dams-new design techniques. Proc Inst Civil Engineers; 1967. p. 433–71.
[21] Peirson WL, Figlus J, Pelles SE, Cox RJ. Placed rock as protection against erosion by flow down steep slopes. J Hydraul Eng 2008;134(9):1370–5.
[22] Peirson WL, Jens F, Pells Steven E, Cox RJ. Placed rock as protection against erosion by flow down steep slopes. J Hydraul Eng 2008;134:1370–5.
[23] Ravindra GHR, Sigtryggsdottir FG, Asbølmo MF, Lia L. Toe support conditions for placed ripraps on rockfill dams- a field survey. Vann 2019;3.
[24] Ravindra GHR, Sigtryggsdottir FG, Lia L. Buckling analogy for 2D deformation of placed ripraps exposed to overtopping. J Hydraul Res 2020.
[25] Siebel R. Experimental investigations on the stability of riprap layers on overtoppable earthdams. Environ Fluid Mech 2007;7(6):455–67.
[26] Sommer P. Überströmbare Deckwerke/ Overtoppable Erosion Protections. Unpublished report No. DFG-Forschungsbericht La 529/8-1 Universita; 1997.
[27] Thielicke W. The flapping flight of birds summary and conclusions PhD Thesis Rijksuniversiteit Groningen; 2014.
[28] Thielicke W, Stamhuis EJ. PIVlab - Time-Resolved Digital Particle Image Velocimetry Tool for MATLAB (Version: 2.02). Published under the BSD license, programmed with MATLAB 7.0.246 (2014): R14; 2014.
[29] Thielicke, William, Stamhuis Eize J. PIVlab – towards user-friendly, affordable and accurate digital particle image velocimetry in MATLAB; 2014.
[30] Thornton CI, Abt SR, Scholl BN, Bender TR. Enhanced stone sizing for overtopping flow. J Hydraul Eng 2014;140(4):06014005–9.
[31] Toledo MÁ, Moran R, Onate E. Dam protection against overtopping and accidental leakage. London: CRC Press/Balkema; 2015.